International Journal of Hydrogen Energy 98 (2025) 576–589

Contents lists available at ScienceDirect

International Journal of Hydrogen Energy

journal homepage: www.elsevier.com/locate/he

Characterisation of double-sided graphene microporous layers for improved polymer electrolyte membrane fuel cell performance

F. Ruscillo [a,*], M.S. Ismail [b], Z.A.R. Gautama [c,d,e], M. Nishihara [c,d,f], K.J. Hughes [a], D.B. Ingham [a], L. Ma [a], M. Pourkashanian [a,g]

[a] Energy Institute, The University of Sheffield, Sheffield, UK
[b] School of Engineering, University of Hull, Hull, HU6 7RX, UK
[c] Next-Generation Fuel Cell Research Center (NEXT-FC), Kyushu University, 744 Motooka, Nishi-ku, Fukuoka, 819-0395, Japan
[d] International Institute for Carbon-Neutral Energy Research (I2CNER), Kyushu University, 744 Motooka, Nishi-ku, Fukuoka, 819-0395, Japan
[e] Graduate School of Engineering Department of Hydrogen Energy Systems Kyushu University 744 Motooka, Nishi-ku, Fukuoka, 819-0395, Japan
[f] International Research Center for Hydrogen Energy Kyushu University 744 Motooka, Nishi-ku, Fukuoka, 819-0395, Japan
[g] Translational Energy Research Centre, The University of Sheffield, Sheffield, UK

ARTICLE INFO

Handling Editor: Shohji Tsushima

Keywords:
Polymer electrolyte fuel cells
Gas diffusion layers
Microporous layers
Carbon black
Graphene
Double-sided MPL coating

ABSTRACT

This study experimentally evaluates the effects of double-sided microporous layer coated gas diffusion layers, comparing conventional Vulcan black with graphene-based microporous layers. Key properties and fuel cell performance were analysed. The results showed that adding graphene improved the in-plane electrical conductivity and increased the gas permeability compared to Vulcan black. Vulcan black microporous layers promoted a more favourable pore size distribution compared to graphene, featuring significant micropores and mesopores in both single and double-sided coatings, while pure graphene produced fewer micropores and mesopores. Contact angle measurements were consistent across all coatings, indicating that wettability depends more on the polytetrafluoroethylene content than on the carbon type. In-situ fuel cell testing demonstrated that a double-sided layer with Vulcan black facing the catalyst layer and graphene facing the bipolar plate performed best under higher humidity conditions by efficiently expelling excess water through the graphene cracks. Conversely, single-sided Vulcan black coatings performed better in low humidity, as their micropore content retained water effectively for membrane humidification.

1. Introduction

Polymer electrolyte membrane fuel cells (PEMFCs) are a highly promising technology for harnessing hydrogen and playing a significant role in the transition to sustainable energy. PEMFCs can efficiently transform the chemical energy stored in hydrogen directly into electricity via electrochemical reactions, yielding only water and heat as its by-products [1]. PEMFCs are a particularly attractive technology due to their high efficiency, ability to operate at a range of low operating temperatures (25 °C – 80 °C), and ease of assembly [2]. PEMFCs are well adapted to facilitate the integration of hydrogen into a range of applications, such as stationary, automotive and portable use [1].

The gas diffusion layer (GDL) is an essential component of the PEMFC. The GDL serves multiple functions within the PEMFC. Firstly, it ensures the even distribution of hydrogen and oxygen to the active sites of the catalyst layer (CL). Additionally, it plays a pivotal role in managing water; ideally, it should remove excess water while keeping the membrane adequately hydrated [3]. Lastly, it provides structural support to the delicate membrane and catalyst layers [4]. Due to the varied tasks it must perform, the GDL is typically made from carbon fibre material, as this best fulfils the multifunctional requirements. A microporous layer (MPL) is conventionally incorporated onto the surface of the GDL. The MPL consists of an ink composed of carbon black and polytetrafluoroethylene (PTFE) [5]. Research has shown that the addition of an MPL to the GDL improves water management within the membrane electrode assembly (MEA) [6–8] and enhances electrical contact between the GDL and the catalyst layer [9,10], consequently, leading to improved overall fuel cell performance [9,11–14].

During the operation of fuel cells, various types of losses occur. Ohmic polarisation losses primarily result from the bulk resistances from

* Corresponding author.
E-mail address: fruscillo1@sheffield.ac.uk (F. Ruscillo).

https://doi.org/10.1016/j.ijhydene.2024.12.094
Received 23 July 2024; Received in revised form 11 November 2024; Accepted 5 December 2024
Available online 11 December 2024

induvial fuel cell components and the contact resistance at the interfaces between these components. Contact resistance occurs because of the differences in structure and morphology of the different components. This leads to transitional regions forming at the boundary of these components, increasing the electrical contact resistance [15]. One area particularly affected by the contact resistance is the GDL. This is because it is positioned between the CL and the bipolar plate (BPP). Numerous studies have explored strategies to reduce contact resistance between the GDL and BPP. These investigations have utilised both simulation-based approaches [16] and experimental methods [17–19] [20].

Chang et al. [18] optimised the double-sided MPL coated GDL without keeping the loading constant. They used SGL 10BA carbon paper with various carbon blacks (Acetylene Black, Black Pearls 2000 and Vulcan XC 72B). An optimal MPL loading of 1.25 mg/cm^2 facing the CL and 0.25 mg/cm^2 facing the BPP was found, leading to a peak power density of 900 mW/cm^2, compared to 750 mW/cm^2 for a single-sided coating. Huang et al. [19] further optimised the MPL configuration under different humidity conditions, finding that a 20 wt% PTFE content was optimal. The double-sided MPL coated GDL showed an 85% increase in peak power density at 13.6% RH, with the lowest ohmic resistances observed at optimal compositions. Due to the robustness and rigorous methodology of this work, the above optimal MPL loadings (i.e. 1.25 mg/cm^2 facing the CL and 0.25 mg/cm^2 facing the BPP) were adopted for this study.

The primary consensus emerging from these research efforts is that the application of an MPL, especially a double-sided MPL-coated GDL, proves effective in decreasing contact resistance. Additional research is required to gain a comprehensive understanding of the potential of double-sided MPL-coated GDLs in reducing contact resistances and reducing the necessity for increased compression in fuel cells. The current studies have predominantly relied on polarisation curves and electrochemical impedance spectroscopy (EIS), offering only limited insights into this matter. Furthermore, these studies have only considered conventional carbon black as the main constituent of the MPL. This study aims to examine the use of the novel material of graphene in the context of the double-sided MPL coated GDL and seeks to further improve the contact resistance between the CL and the BPP.

Novel material usage in MPL fabrication is becoming more widespread, as they are shown to increase the capabilities of the MPL. In particular, graphene shows great promise [21]. The aim of using novel materials is to take advantage of their natural properties and increase the performance of the MPL, in particular, reducing contact resistance, improving bulk conductivity and enhancing mass transport processes. Graphene as a novel material for the MPL has recently been a subject of exploration [22–29]. Graphene consists of a two-dimensional monolayer of graphitic carbon atoms. Graphene has excellent properties such as high electrical and thermal conductivity, large surface area, chemical stability and mechanical strength [23,30,31].

Leeuwner et al. [24] highlighted the contact resistance between the MPL and the CL as a key issue affecting electrical conductivity. They compared various MPL materials, including conventional carbon black, graphene foam, and graphene sheets, finding that graphene foam improved the electrical conductivity due to its high conductivity and strong interfacial adhesion. At mid-range current densities, graphene achieved a peak power density of 362 mW/cm^2 versus 334 mW/cm^2 for carbon black. However, graphene was less effective at higher current densities due to difficulties with water expulsion. A composite MPL of graphene and carbon black performed better at high humidity by optimising water management.

Studies by Ozden et al. [25] and Najafabad et al. [23] confirmed graphene's advantages in electrical conductivity and water management. Ozden found graphene-based MPLs had higher in-plane conductivity and improved power density under low to medium humidity, showing a 55% increase in peak power density over Ketjenblack. In comparison with Vulcan black, graphene's unique flake structure

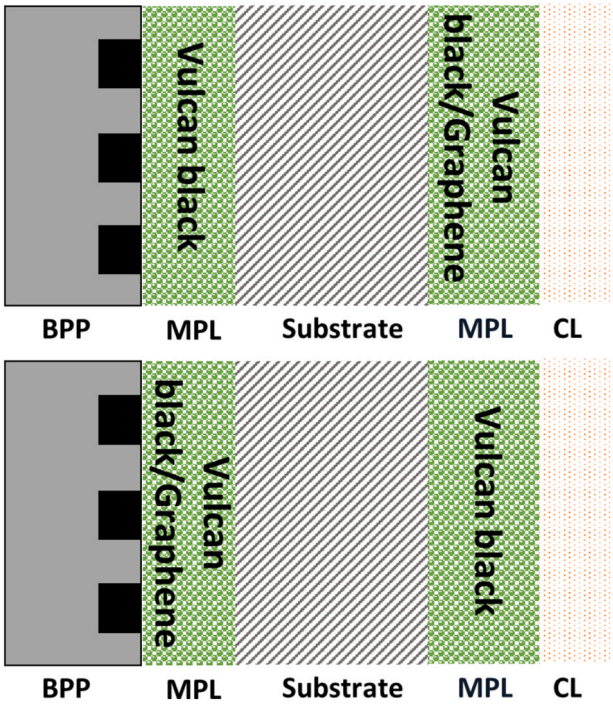

Fig. 1. The two configurations used for double-sided MPL coated GDL.

doubled in-plane conductivity, with 43% higher peak power density under humid conditions. Najafabad et al. observed that a graphene-carbon black composite MPL reduced ohmic losses and maintained membrane hydration across a wide range of humidities. However, graphene did not perform as well as the conventional MPL under high humidity conditions. Mariani et al. [27] compared different graphene particles, with medium-sized nanoplatelets performing best across humidity levels, although flooding was still an issue. Adding carbon black increased the micropores, while graphene facilitated mesopore and macropore formation, improving the performance at low humidity. Lee et al. [29] optimised graphene-Vulcan black MPLs, finding higher graphene content ($\geq$50 wt%) enhanced water management at high humidity, while 30 wt% graphene significantly boosted the in-plane electrical conductivity of the MPLs. Overall, these findings suggest graphene-based MPLs can improve fuel cell performance through enhanced electrical conductivity and tailored water management.

The double-sided MPL configuration is a novel approach that offers new insights into fuel cell design. This arrangement has shown potential to significantly improve the performance by better managing mass transport and reducing contact resistance across different operational conditions. The study further advances the understanding of the structural and electrochemical properties of double-sided MPL coated GDLs and provides a foundation for future optimisation. The growing interest in enhancing the GDL and reducing contact resistance underscores the potential of novel materials, notably graphene, due to its improved surface contact and higher electrical conductivity. However, graphene's application in the MPL is still in its early stages and is limited in scope. More research is needed to determine the optimal graphene quantities for MPL, particularly in high-humidity conditions where efficiency may diminish. Surprisingly, there is a lack of studies on the impact of novel materials, especially in the context of a double-sided MPL-coated GDL. The double-sided MPL architecture has demonstrated improved PEMFC performance [20,32–36] and graphene could further enhance this. Moreover, the double-sided MPL-coated GDL exhibits better performance across various humidity conditions compared to conventional MPLs. Investigating how a graphene-based double-sided MPL coated

Table 1
Cathode GDL samples prepared for the investigation.

Abbreviation	MPL Material	Total MPL Loading Side 1 (CL) (mg/cm^2)	Total MPL Loading Side 2 (BPP) (mg/cm^2)	Graphene % in the MPL	Side the Graphene is Applied to
Single coated					
SVB	Vulcan black	1.25	–	–	–
SVBG	Vulcan black/ Graphene	1.25	–	50%	–
SG	Graphene	1.25	–	100%	–
Double coated					
DVB	Vulcan black	1.25	0.25	–	–
D_VBG50_VB100	Vulcan black/ Graphene	1.25	0.25	50%	Side 1
D_VB100_VBG50	Vulcan black/ Graphene	1.25	0.25	50%	Side 2
D_VBG50_VBG50	Vulcan black/ Graphene	1.25	0.25	50%	Side 1 and 2
D_G100_VB100	Vulcan black/ Graphene	1.25	0.25	100%	Side 1
D_VB100_G100	Vulcan black/ Graphene	1.25	0.25	100%	Side 2
DG	Graphene	1.25	0.25	100%	Side 1 and 2

GDL performs under different relative humidities is an intriguing avenue for research. Mixing graphene with carbon black has the potential to optimise the MPL, as previous studies have shown. Additionally, the unique architecture of the double-sided MPL-coated GDL could compound the advantages of a novel structure with a novel material, further improving PEMFC performance.

2. Materials and methodology

This investigation will systematically analyse the double-sided MPL coated GDL at the cathode side, to assess the overall performance resulting from the introduction of graphene. Also, it will be identified, if applicable, on which side of the GDL that graphene exhibits the most significant performance improvement. As detailed in Fig. 1, one side of the double-sided MPL coated GDL will be maintained constant with the Vulcan black, whilst the other side will change composition (Vulcan black, graphene and Vulcan black/graphene). This approach is designed to facilitate an in-depth examination of the consequences arising from the introduction of graphene into the MPL.

2.1. Fabrication procedure

The GDL used for all of the cathode samples was Toray Carbon Paper (TGP-H-060 PTFE 10 wt %) (Fuel Cell Earth, Woburn, MA, USA) with a thickness of 190 μm. The MPL coatings consisted of Vulcan Black XC 72 R (Sigma Aldrich®, Gillingham, UK) and graphene nanoplates (Sigma Aldrich®, Gillingham, UK). The categories of samples that were used for the investigation are shown in Table 1. The anode side GDL was kept constant: Toray Carbon Paper (TGP-H-060 PTFE 10 wt %) was used. The loadings of each side of the MPL were kept constant at a 1.25 mg/cm^2:0.25 mg/cm^2 ratio as detailed in the previous study [36]. The PTFE content in all MPLs will be kept constant at 20 wt %.

A mixture was prepared, consisting of 800 mg of Vulcan black (Sigma Aldrich®, UK), 200 mg of a 60 wt% PTFE dispersion (Sigma Aldrich®, Gillingham, UK), methylcellulose (Sigma Aldrich®, UK), and 21.6 μg of Triton X 100 (Sigma Aldrich®, UK). This mixture was blended with deionised water and stirred at 800 rpm for 30 min until a viscous consistency was achieved. This quantity of MPL ink was enough to create up to five samples of double-sided MPL-coated GDLs. To create the

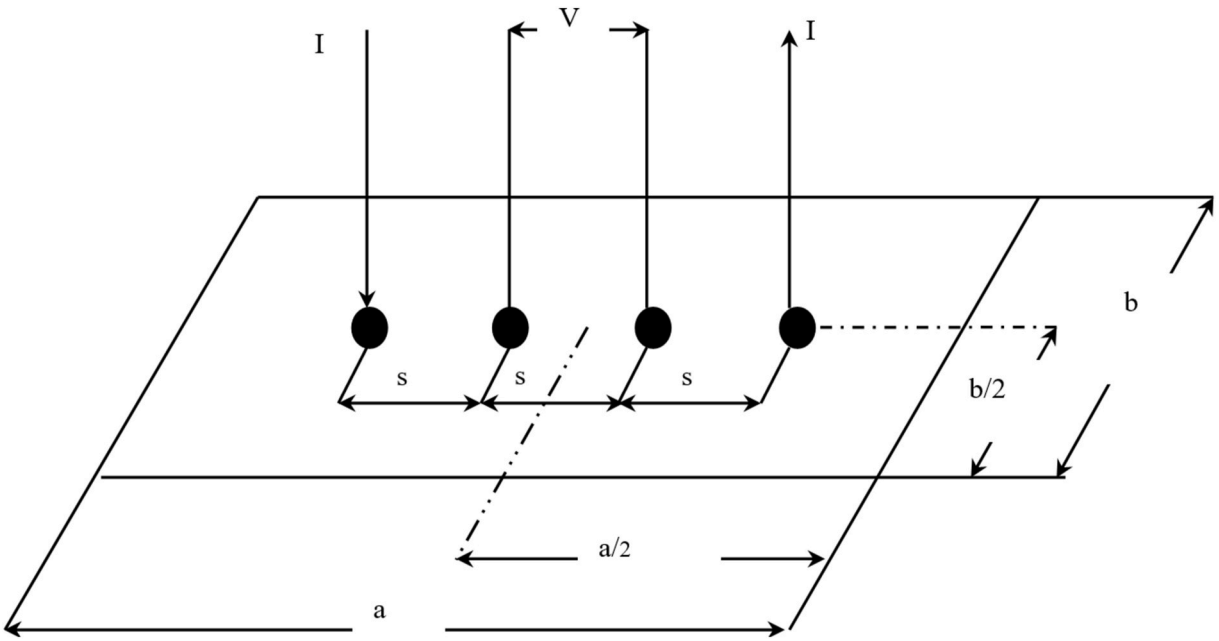

Fig. 2. In-plane electrical conductivity experimental set-up [10].

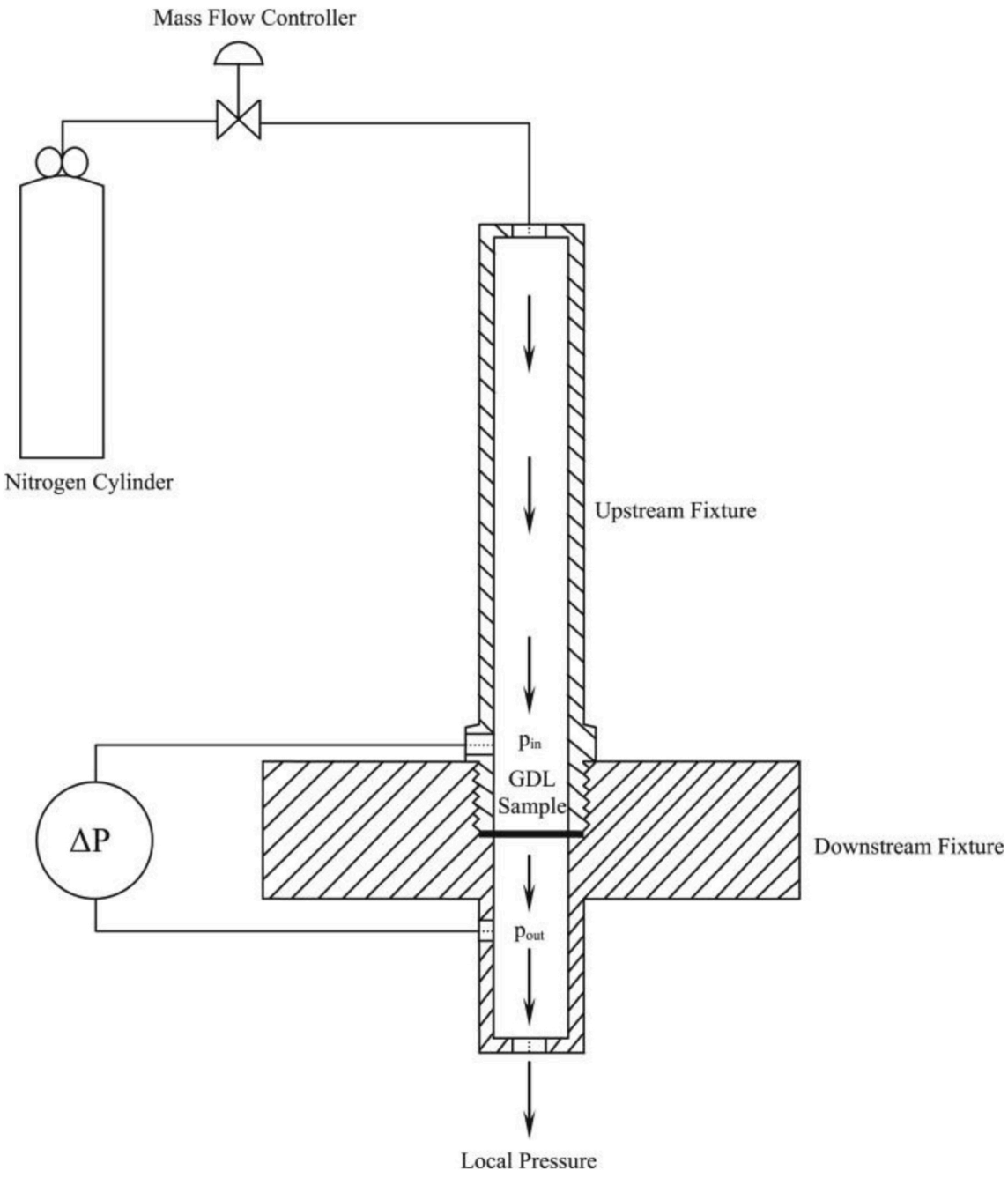

Fig. 3. Experimental setup used to measure through-plane permeability [39].

graphene based MPL, the same procedure was followed, but with the substitution of Vulcan black for graphene nanoplates. In the case of the Vulcan black/graphene mixture, these were mixed in a 1:1 ratio. The MPL ink was then applied to Toray carbon paper after it was secured to a hot plate set at 90 °C. The 1.25 mg/cm^2 loading was applied first using the doctor blade apparatus. If the sample was a double-sided MPL coated GDL, it was then flipped and the 0.25 mg/cm^2 loading of MPL was subsequently applied. The samples were then sintered in a nitrogen-rich environment at 1 bar and 350 °C, for half an hour. Each category described in Table 1 was comprised of 5 samples with dimensions of 7 cm × 2.5 cm.

2.2. Preparation of the membrane electrode assembly

The catalyst ink was prepared by combining Pt/C (TEC10E50E, lot 1019–8581, 46.8 wt. Pt %, Tanaka, Japan), with 5 wt % Nafion solution (Wako, Japan), deionised water, and super-dehydrated ethanol (99.5 vol %, Wako, Japan). To ensure thorough mixing, the catalyst ink was subjected to 30 min of sonication using an Ultra Sonic Homogeniser UH-600 from SMT Corporation. For the assembly of the MEA, Nafion 212 membranes were carefully positioned on a movable-hot plate and masked, leaving an exposed area of 1 cm^2. The catalyst ink was then sprayed directly onto the Nafion membrane in order to achieve a catalyst loading of 0.3 mg Pt/cm^2 with a Nafion content of 28 wt %, at both the anode and the cathode sides. This spraying process was carried out using the pulsed spray mode of an automated spraying device (Nordson K.K., C3J). Finally, the resulting MEAs were placed in a hot press at 132 °C and 0.3 kN for a duration of 180 s, using the Sinto Digital Press CYPT-10. This step ensured the proper bonding and integration of the components.

2.3. In-plane electrical conductivity

The GDL samples' in-plane conductivity was experimentally assessed through the utilisation of the 4-probe technique, as outlined by Smits [37]. This method employs four probes positioned equidistantly, as depicted in Fig. 2.

When using the Smits method, the correction factor needs to be obtained which is based on two geometric ratios. The sample's length and width (a/b) give the initial ratio, while the sample's width and the spacing between the probes (b/s) give the second ratio [37]. In this investigation, these ratios were determined to be 3 and 1.25, respectively. Consequently, this gave a correction factor of 0.9973. The resistivity, denoted as ρ, can then be computed using the subsequent formula [37]:

$$\rho = CtR \tag{1}$$

Where resistivity C is the correction factor, t is the thickness of the sample and R is the electrical resistance. Following this, the electrical conductivity, σ, of the GDL can be found by the reciprocal of the resistivity:

$$\sigma = \frac{1}{\rho} \tag{2}$$

A micrometre was used to obtain the thickness of the samples. Notably, the thickness of the GDL varied among the different samples. Additionally, within each sample, slight thickness variations were observed at different positions. To account for this variability, thickness measurements of each GDL sample were taken at five evenly spaced positions and then an average value was calculated. Subsequently, the GDL samples were secured to an insulating plate. The copper electrodes measuring 10 mm × 10 mm × 5 mm were positioned onto the GDL sample. Using a high-precision ohmmeter (RS Pro 804, RS Components, London, UK) with a resolution of 0.01 mΩ, electrical resistance measurements of the samples were taken. Also it is important to note that the through-plane conductivity of the MPLs is likely to be similar to the in-plane conductivity, and this is due to the uniformity of the MPL structure.

2.4. Permeability

The permeability of the samples can be estimated by using Darcy's law:

$$Q = \frac{kA\Delta P}{\mu L} \tag{3}$$

The flow rate (Q) through a porous material equals the product of the permeability (k), cross-sectional area (A), and pressure drop (ΔP), all divided by the product of the sample's viscosity (μ) and its thickness (L) [38]. To help calculate the permeability of the samples, the experimental setup displayed in Fig. 3 was used [39].

The configuration of the experimental setup consists of two fixtures: one fixture is placed upstream and the other downstream. This enables controlled airflow through the sample and measurement of the resulting pressure drop. The sample itself is prepared using a circular punch with a 25.4 mm diameter, but when placed between the fixtures, only a 20 mm diameter area is exposed to the airflow. An HFC-202 flow controller is employed to control the flow rate of nitrogen gas, providing a range of 0.0–0.1 standard litres per minute (SLPM). Measurement of the pressure difference across the sample is carried out using a PX653 differential pressure sensor, capable of measuring within a range of ±12.5 Pa. Utilising Darcy's Law (Equation (3)), the gas permeability of the sample can be calculated. This permeability is determined for each sample at different flow rates, and an average value is taken. The entire process is replicated for all five samples within each category, as outlined in Table 1.

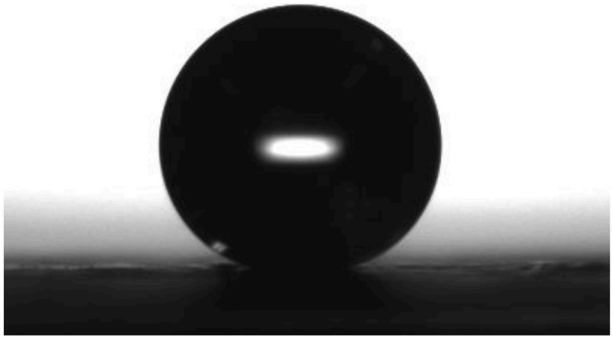

Fig. 4. A typical water droplet on a surface of a GDL sample.

2.5. Pore size distribution

Mercury intrusion porosimetry (MIP) is a widely used technique for determining pore size distribution in materials. In the MIP process, a small sample of the GDL is immersed in mercury. Initially, due to mercury's high surface tension, it does not easily penetrate the GDL's pores. The pressure on the mercury is then increased incrementally, causing it to gradually infiltrate the GDL's pores, starting with the larger ones and progressively filling smaller ones [40]. The resulting pore size distribution is determined by measuring the intrusion pressure of the mercury, which is inversely related to pore size. It is important to note that this method assumes the pores to be cylindrical and does not account for closed pores. However, for materials such as carbon papers, this assumption is deemed acceptable [41].

Pore size distribution plays a crucial role in understanding the mass transport mechanisms of gas and liquid water within the porous GDL media [42]. Additionally, it is a key parameter for modelling and optimising mass transport processes in fuel cells [40]. In general, the pores in a GDL can be classified into three main categories based on their radii: micropores (less than 50 nm), mesopores (50–7000 nm), and macropores (larger than 7000 nm) [43]. Macropores predominantly constitute the GDL [44], but the introduction of an MPL influences the pore size distribution of a sample by increasing the presence of micropores and mesopores. Macropores primarily facilitate gas diffusion, while micropores play a crucial role in liquid water removal [45,46].

2.6. Contact angle

The contact angle serves as a measure of a material's wettability. When the contact angle is less than 90°, the material is classified as hydrophilic. Conversely, if the contact angle exceeds 90°, the material is considered hydrophobic [47]. To determine the contact angle of the samples, the sessile drop (DMs-401, Kyowa Interface Science Co., Ltd, Japan) method was employed. In this method, individual water droplets were carefully deposited onto the surface of the GDL sample (Fig. 4). High-resolution photographs were then captured within the first 3 s after the droplets settled on the surface; this is to account for the transient behaviour of the water [45]. Subsequently, contact angle values were measured, with each sample undergoing ten measurements, and then an average value was calculated.

2.7. Morphology

Scanning electron microscopy (SEM) was utilised to scrutinise the morphological characteristics of the GDL samples. This enabled the analysis of the surface morphology and fibre structure of the samples. SEM micrographs play a significant role in evaluating GDL morphology and assessing fuel cell performance [2,22,46]. In this analysis, GDL samples were first cut into 1 cm^2 squares. These squares were then securely attached to SEM stubs using carbon tape and placed on the specimen stage. The SEM (JEOL - Model JSM-6010LA), operating at 10

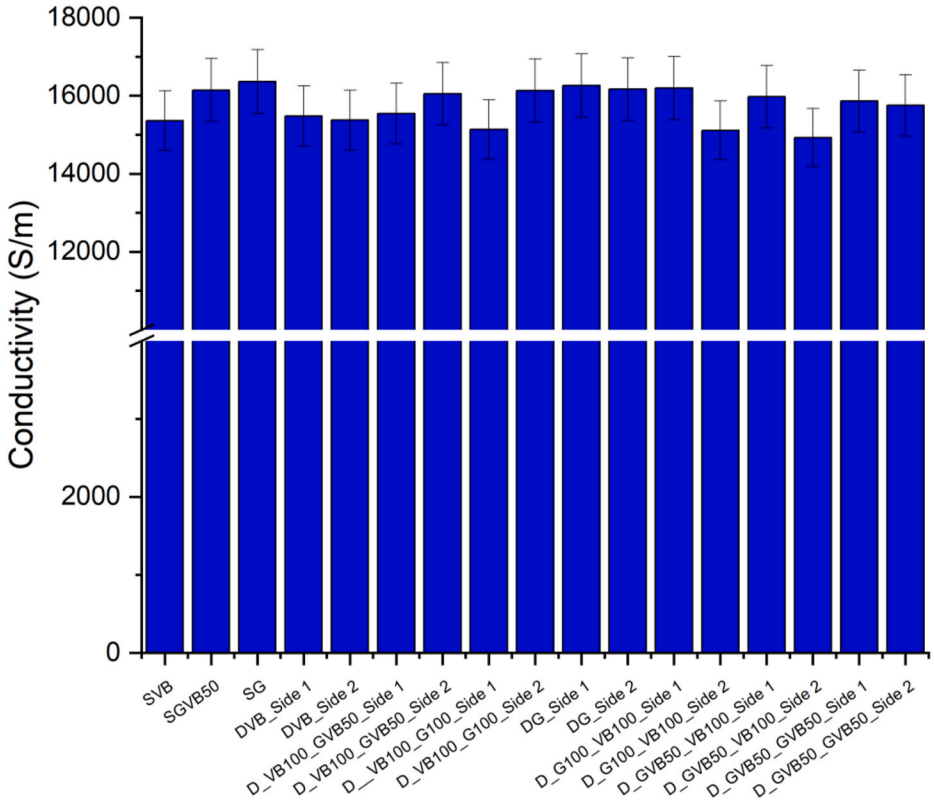

Fig. 5. In-plane electrical conductivity of the MPL samples.

kV, facilitated the examination of each sample at various magnifications.

2.8. *In-situ fuel cell testing*

A 1 cm^2 active area single cell was used for the testing from the Japanese Automotive Research Institute (JARI). The fuel cell was fitted

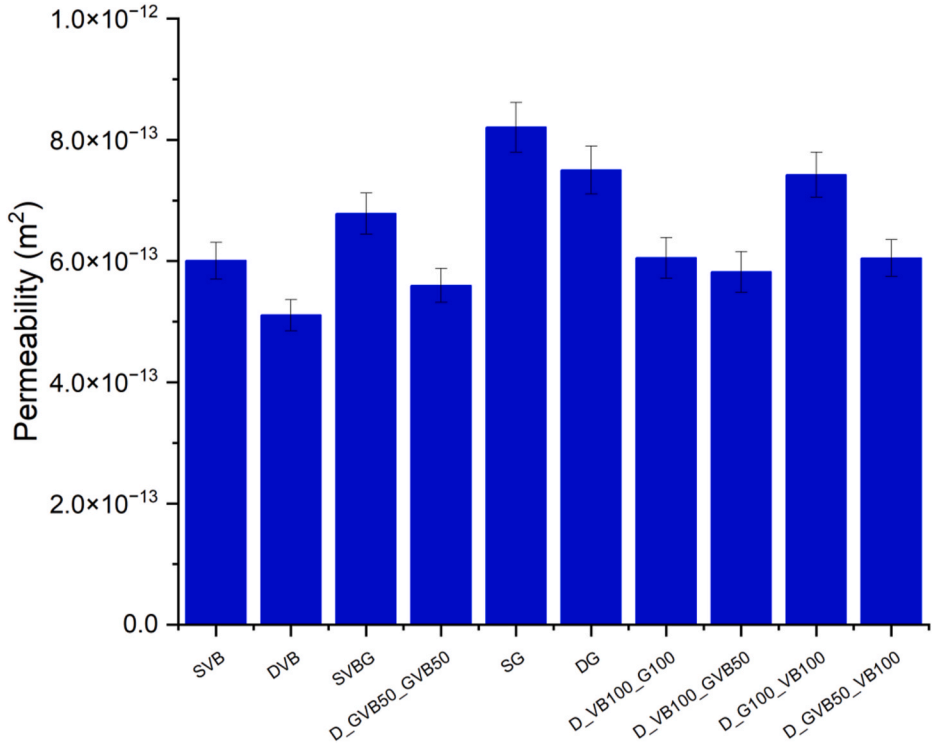

Fig. 6. Permeability of GDL samples.

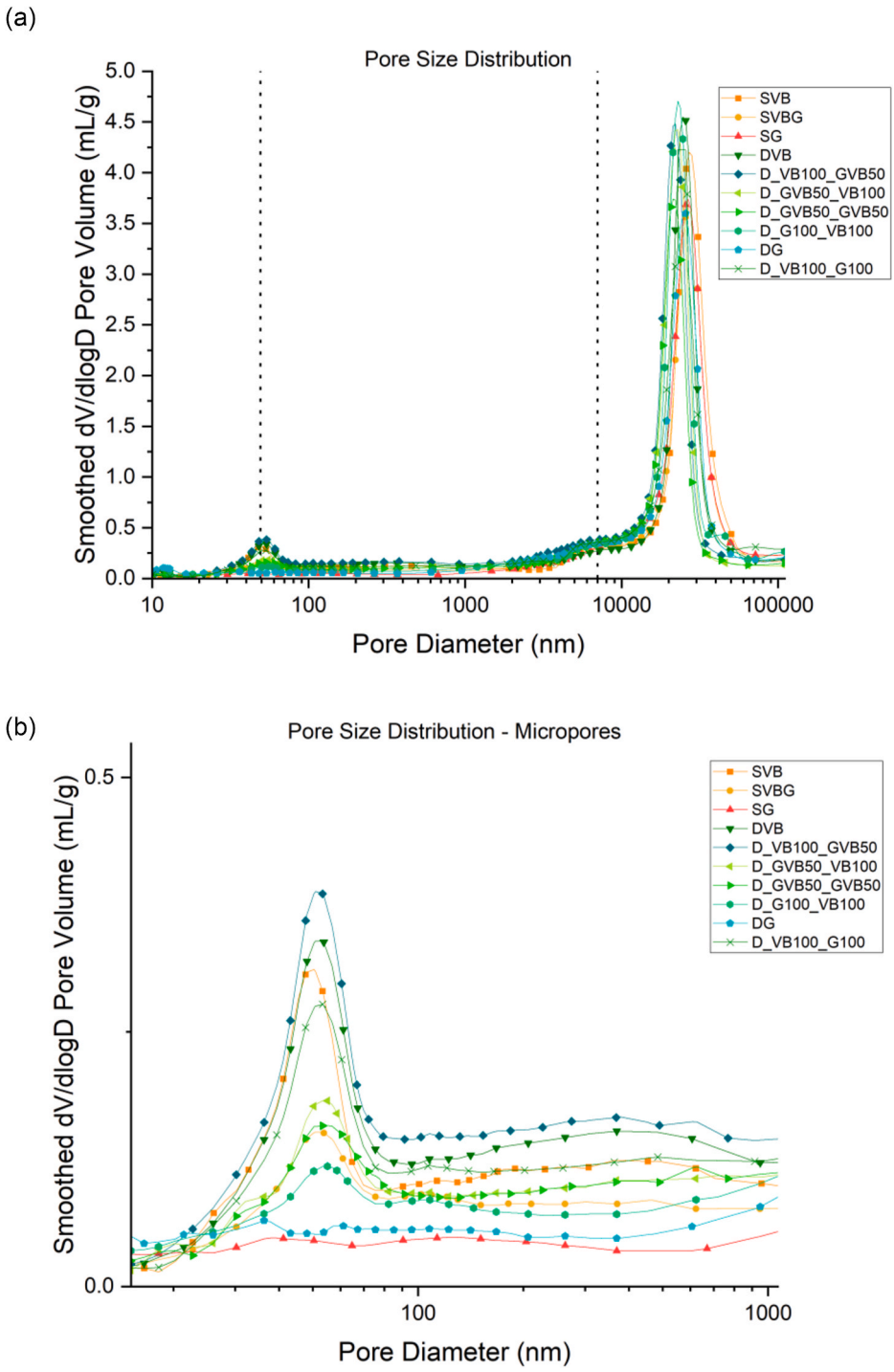

Fig. 7. (a) Pore size distribution of the samples and (b) zoomed-in image highlighting micropores and mesopores ranges of the samples.

with graphite bipolar plates with serpentine type flow fields. The fuel cell operated under counter flow conditions, with constant volumetric flow rates of 0.139 L/min for hydrogen at the anode and 0.332 L/min for oxygen at the cathode.

To ensure proper control of the experimental conditions, a fuel cell test station (AUTOPEM-CVZ01, Toyo Corporation, Japan) was employed. This test station allowed for precise regulation of humidification, cell temperature, and gas flow throughout the testing process. An electrochemical interface impedance analyser (Solartron SI-1287) was used to measure the polarisation curves. Before conducting the in-situ measurements, the cell underwent a conditioning process at a voltage of 0.6 V for a duration of 16 h.

The fuel cell was set to an operating temperature of 80 °C. The inlet gases (hydrogen and air) were also set at 80 °C. The fuel cell was then humidified via the inlet gases. Once this had been done, the polarisation and EIS data was subsequently collected for four different relative humidity (RH) conditions: 25%, 50%, 75% and 100%. These varying humidity conditions allowed for a comprehensive assessment of the fuel cell's performance across different humidity levels.

3. Results and discussion

3.1. In-plane electrical conductivity

In-plane electrical conductivity of the samples are displayed in Fig. 5. Note that the error bars in this figure (and other figures) represent the 95% confidence intervals around an average value of the 5 samples that were measured. It can be seen that when graphene is introduced into the MPL, it leads to an enhancement in its electrical conductivity. This increase in electrical conductivity can reach a difference of approximately 800 S/m when compared to the conductivity of the pure Vulcan black (SVB, DVB) samples, emphasising graphene's conductive properties. This outcome aligns with expectations, given the excellent electrical conductivity of graphene, which is widely documented in scientific literature [22]. Therefore, it is expected that the inclusion of graphene in the MPL composition consistently enhances the in-plane electrical conductivity across all MPL samples that contain graphene. It is particularly interesting observation, that when graphene is incorporated into a 50% composite with Vulcan black (SVBG, DVB100_GVB50, D_VB100_VBG50, D_VBG50_VBG50), the resulting electrical conductivity shows a comparable improvement to that observed with the pure graphene samples (SG, DG, D_G100_VB100, D_VB100_G100). This suggests that even a modest addition of graphene can elevate the conductivity levels to be on par with those achieved by pure graphene. Furthermore, it's worth noting that the variation in electrical conductivity is not so much influenced by whether the material is double-sided or single-sided, but rather by the type of carbon used in the MPL. This observation underscores the significance of the carbon source in determining electrical conductivity of an MPL. Additionally, the through-plane electrical conductivity of the MPLs is highly expected to be similar to the in-plane conductivity, due to the uniformity of the MPL particle structure.

3.2. Gas permeability

The permeability of the gas diffusion layer is intricately tied to its physical structure and morphology, particularly in relation to porosity and pore size distribution [10]. Firstly, it can be seen in Fig. 6 that the double-sided configuration exhibits lower permeability compared to the single-sided configuration. This outcome aligns with expectations, as the addition of an extra layer of MPL facing the BPP not only increases the thickness of the GDL but also fills in the surface pores of the GDL substrate. Specifically, double-sided Vulcan black (DVB) has a difference of 0.9×10^{-13} m^2 decreasing permeability, compared to single-sided Vulcan black (SVB). Similarly double-sided graphene (DG) experiences a decrease of 0.7×10^{-13} m^2, compared to single-sided graphene (SG). Additionally, the composite MPLs comprised of Vulcan black and graphene (DVB100_GVB50, D_VB100_VBG50, D_VBG50_VBG50), exhibit a similar decrease in permeability of around of 1×10^{-13} m^2 compared to the single-sided MPL samples (SVB, SVBG, SG).

The second significant observation is that the introduction of graphene enhances the sample's permeability. For example, the permeability of single-sided graphene (SG) is higher than that of single-sided Vulcan black (SVB) increasing by 2.2×10^{-13} m^2. Similarly, the double-sided graphene sample (DG) has a greater permeability, by 2.4×10^{-13} m^2, compared to the double-sided Vulcan black (DVB). This phenomenon can be attributed to the morphology of graphene, which features more surface cracks and generally larger pores compared to Vulcan black. This will be elaborated on when exploring the morphology and pore size distribution of the samples. It can also be observed that the GDLs with a more predominant type of carbon in it, will behave more like the pure carbon counterpart. For example, GDLs with a MPL configuration that contains more graphene than Vulcan black (e.g. DG, D_G100_VB100) will have a permeability more similar to the pure graphene samples than the pure Vulcan black samples (DVB). This would also suggest that permeability is primarily influenced by the type of carbon used rather than the double or single sided structure.

Table 2
Porosity of the GDL samples.

Sample Type	Porosity (%)
SVB	72.8
SG	73.8
SVBG	73.9
DVB	71.3
D_VB100_GVB50	73.6
D_GVB50_VB100	72.8
D_GVB50_GVB50	73.1
D_G100_VB100	72.9
DG	73.2
D_VB100_G100	72.5

3.3. Pore size distribution

Fig. 7 shows the pore size distribution of the samples. Firstly, it is important to highlight that there is a broad spectrum of pore sizes; literature has identified the anisotropic microstructure of the GDL which gives rise to the range of pore sizes [48]. In order to delineate between the significant pore sizes, Fig. 7 has been segregated into three distinct categories of pores: micropores (<50 nm), mesopores (50–7000 nm), and macropores (7000 nm), aligning with the classifications discussed in above. Assessing the comparison between Vulcan black and graphene samples when it comes to the pore size distribution shows some significant results.

Vulcan black as an MPL material, tends to create a greater number of micro and mesopores in comparison to the graphene based samples. Specifically, when examining single-sided graphene (SG) and double-sided graphene (DG), it becomes evident that they possess the lowest quantity of micropores among the samples. Contrastingly, the samples containing pure Vulcan black (SVB and DVB) display the highest proportion of micropores. Moreover, a clear trend can be seen, where the introduction of more Vulcan black into the MPL, leads to an increase in micropores, as demonstrated by DVB and D_VB100_GVB50, which exhibit the highest micropore counts and have the highest content of Vulcan black. The increase in the quantity of micropores evidently has an impact on the transport of reactant gases and liquid water within the GDL, thus leading to consequential effects on the fuel cell's performance, which will be discussed in further detail in the next sections.

The type of MPL configuration (single-sided and double-sided coating) also displays some differences. Examining the pure Vulcan black samples, the DVB shows an increase in the quantity of micropores compared to the SVB samples. This trend is also present in the SG and DG samples. As the second coating of MPL is applied to the GDL, this creates more micropores as more of the larger pores of the GDL are filled in with the MPL ink.

The porosity values displayed in Table 2, do not display much of a variation between the types of carbon black particles used for the MPL. They also do not highlight any differences between the single-sided or double-sided configuration.

3.4. Contact angle

The wettability of a GDL plays a pivotal role in overall PEMFC performance, especially with respect to liquid water management. The wettability of a GDL depends upon a combination of the material's physical properties and the surface structure. These factors determine the interactions occurring between the MPL surface and water droplets. The results of these measurements, shown in Fig. 8, revealed a consistent trend across all GDL samples. Each sample was hydrophobic, exhibiting a contact angle greater than 130°. The minor variations observed in the measured contact angles of MPLs containing graphene, Vulcan black and the composite mixture of Vulcan black and graphene, suggests that the primary factor governing wettability is the PTFE content which was made constant at 20 wt %. This consistency in PTFE content implies that

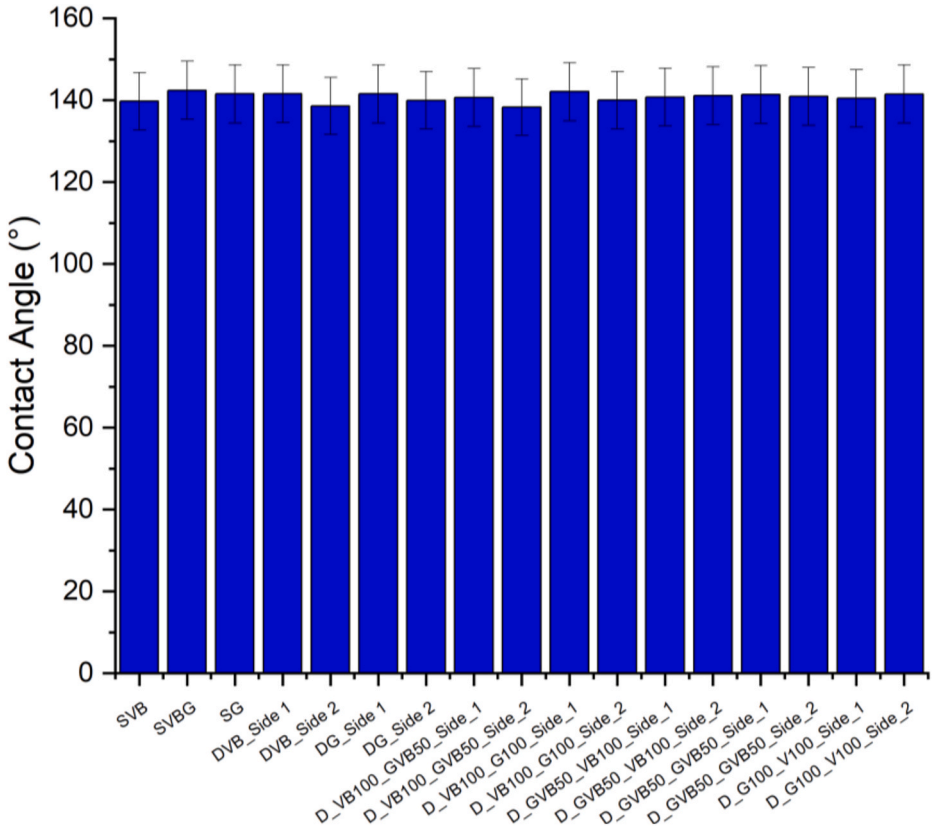

Fig. 8. Contact angle measurements of the GDL samples.

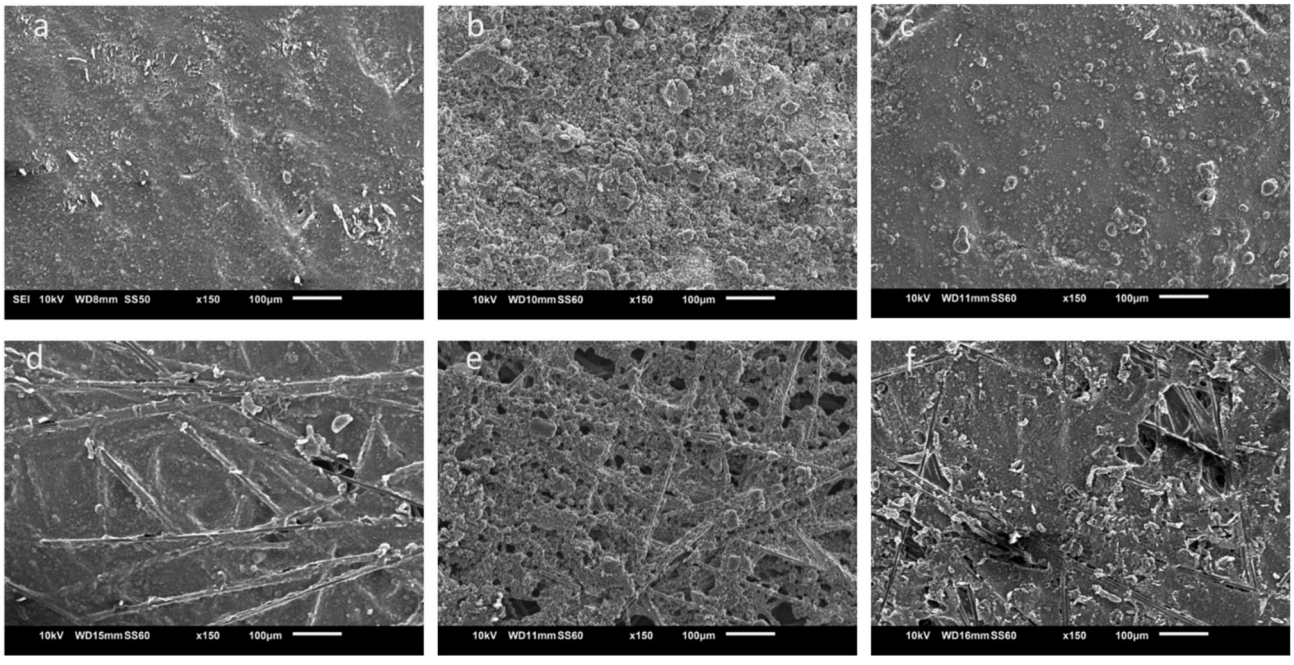

Fig. 9. SEM images for (a) Vulcan black 1.25 mg/cm^2 loading, (b) Graphene 1.25 mg/cm^2 loading, (c) Vulcan black/Graphene 1.25 mg/cm^2 loading, (d) Vulcan black 0.25 mg/cm^2 loading, (e) Graphene 0.25 mg/cm^2 loading, (f) Vulcan black/Graphene 0.25 mg/cm^2 loading.

it plays a dominant role in dictating the wettability characteristics of these MPLs, rather than the type of carbon particles used in the fabrication of the MPL.

3.5. Morphology

Scanning Electron Microscopy (SEM) was employed to visualise the surface structure and morphology of the different MPL surfaces. Fig. 9 shows a series of SEM micrographs that compare the surface structures

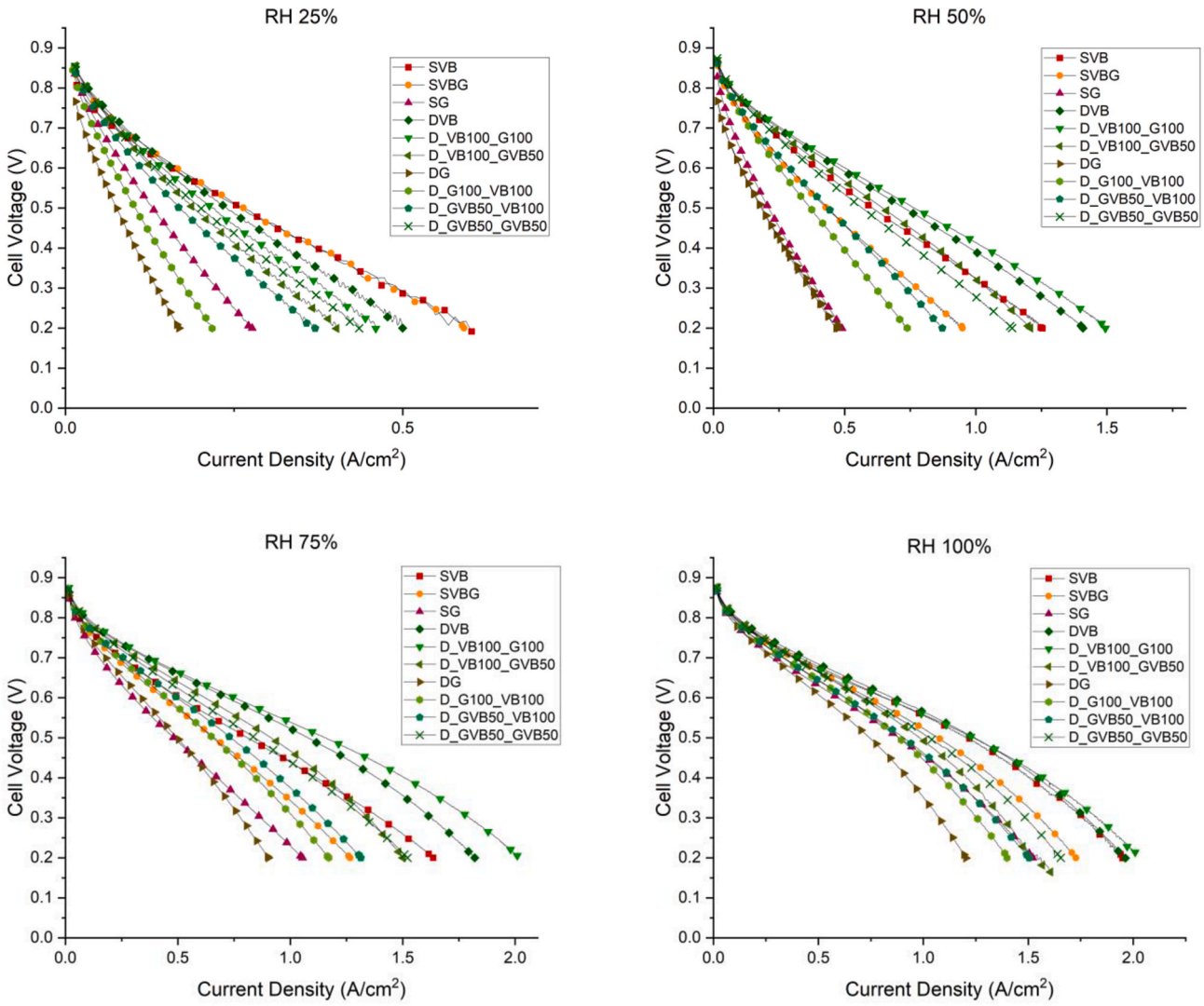

Fig. 10. The polarisation curves of the fuel cell operating with the investigated samples at various humidity conditions (RH 25%, RH 50%, RH75% and RH 100%). The fuel cell operated at a temperature of 80 °C under atmospheric pressure with a 0.139 L/min flow of hydrogen at the anode and 0.332 L/min flow of air at the cathode.

of Vulcan black, graphene, Vulcan black/graphene for both the 1.25 mg/cm^2 loading and the 0.25 mg/cm^2 loading. These images reveal striking disparities in surface structure and morphology between the MPLs containing Vulcan black and those that incorporate graphene. These distinctions are contingent on the physical attributes of the different carbon materials. Vulcan black gives a smooth surface while graphene gives a much rougher surface with clusters of carbon which form on the surface. Also notable, is the graphene MPL structure has more micro-cracks on the surface. MPL surface cracks emerge naturally during the fabrication process. This arises as a result of solvent evaporation during the thermal treatment phase [49]. Such surface cracking is a common trait of MPLs based on carbon black and has been a subject of study in literature [49,50]. With regards to the graphene MPLs, these cracks are more pronounced compared to the Vulcan black MPLs. This could be due to the agglomeration of the graphene particles which means it does not fully spread over the surface of the substrate, thus lending itself to be more susceptible to surface cracks.

On the side facing the BPP, with the 0.25 mg/cm^2 loading, the carbon fibres of the GDL substrate can be easily seen, for all samples. This is expected as the lower the loading of the MPL, the lower the thickness of the coating on the surface. The pure Vulcan black exhibits a smooth surface much like in the 1.25 mg/cm^2 loading, the smooth surface allows for the effective filling of the substrate surface pores, despite the exposure of the carbon fibres. The graphene on the other hand, as it clusters, occupies fewer of these surface pores, allowing the substrate to remain more visible, with visibly larger pores present. The Vulcan black/graphene composite, features a smooth surface, similar to the pure Vulcan black. However, there are small clusters of carbon forming on the surface, similar to the pure graphene samples.

3.6. *Fuel cell performance*

Fig. 10 displays the polarisation curves for the samples, at 25%, 50%, 75% and 100% RHs. Fig. 11 shows the corresponding power density curves and Fig. 12 displays the EIS data. Firstly, it can be seen that in general, the double-sided configuration exhibits better fuel cell performance compared to the single-sided counterparts, at relative humidities of 50%, 75%, and 100%; this is (given that the fuel cell is not membrane resistance limited) due to presence of MPLs facing the bipolar plates and consequently better electrical contact with these plates. Conversely, the single-sided configuration outperforms the double-sided samples at 25% RH. This can be observed in the polarisation curves shown in Fig. 10, where the single sided coatings (SVB and SVBG) both have better performance at higher current densities in the concentration polarisation

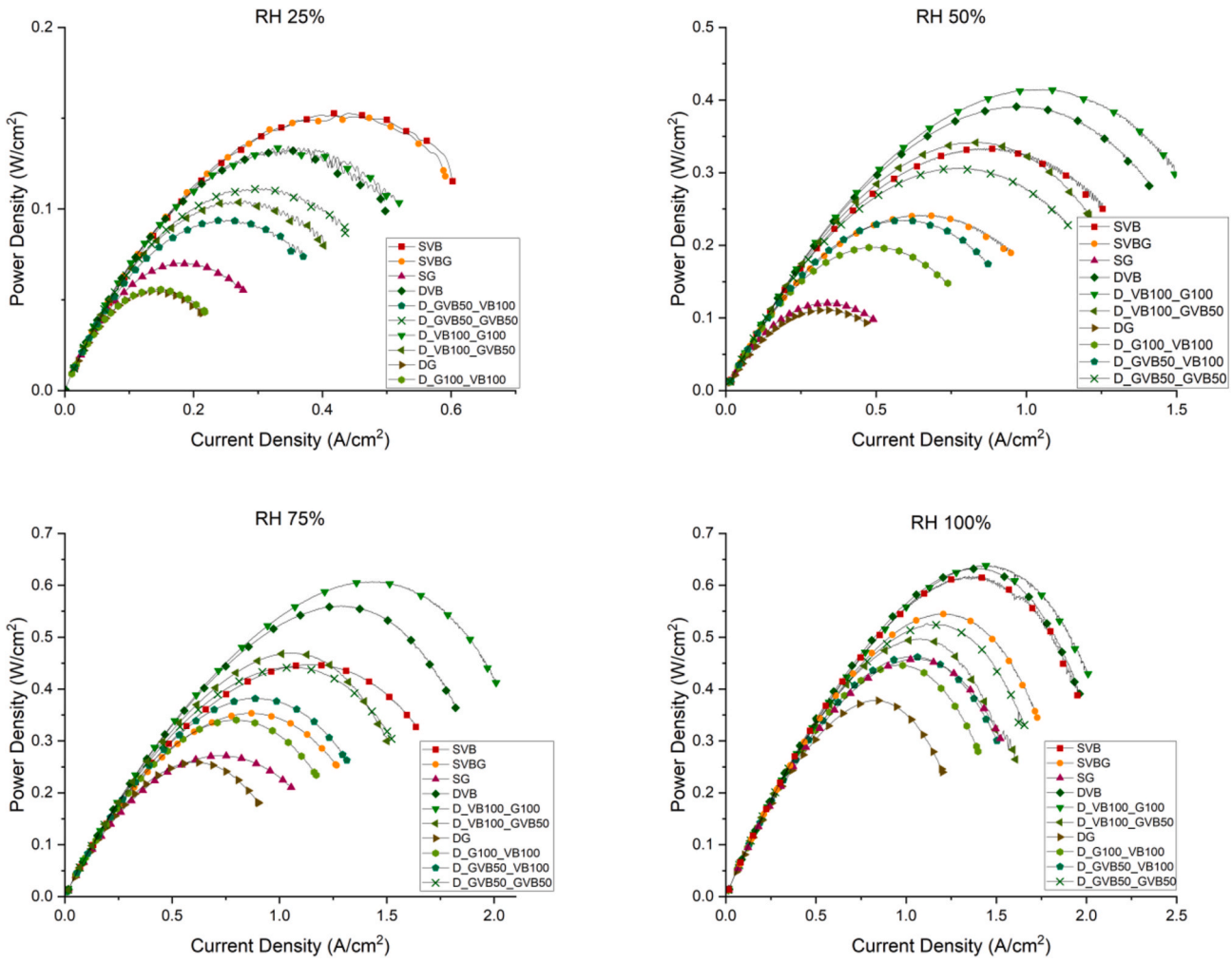

Fig. 11. The power density curves of the fuel cell operating with the investigated samples at various humidity conditions (RH 25%, RH 50%, RH75% and RH 100%).

region of the fuel cell. The better performance of the single-sided SVB and SVBG can be attributed to a lower diffusion path (i.e. lower mass transport resistance), due to the samples having one less coating of MPL compared to the double-sided MPL coated GDLs.

Considering the single-sided samples (SVB, SVBG, SG) at 25% RH, it can be seen that there is a trend where the SVB and SVBG perform the best and SG performs the worst. This could be attributed to the fact that the SVB and SVBG samples contain a high amount of micropores (Fig. 7) that is necessary to retain water required for membrane humidification at relatively low humidity conditions [29]. This is corroborated by the EIS measurements at 25% RH (Fig. 12) that show that the SVB and SVBG samples, compared to SG, have less ohmic resistance (represented by the left intercept of the semicircle with the x-axis) signifying better membrane humidification and consequently less membrane resistance.

Among the samples, D_VB100_G100 demonstrate the best overall performance, closely followed by the DVB sample. This could be attributed to the fact that, under relatively high humidity conditions, the double-sided MPL coating lowers the contact resistance with the BPP. Furthermore, these samples (D_VB100_G100 and DVB) have a good balance of micropores and mesopores, which is important for draining excess liquid water at high current densities, particularly for the side facing the catalyst layer. Research has shown that a combination of micropores and mesopores improves the water removal capabilities of a GDL in high humidity conditions [29]. The EIS measurements of the above samples (Fig. 12) at high relative humidities (≥50%) show that they, compared to other samples, demonstrate less membrane resistance and less charge transfer resistance (represented by the diameter of the semi-circle). This signifies both adequate membrane humidification and mitigated water flooding at the catalyst layer. Additionally, the D_VB100_G100 sample, which contains graphene facing the BPP, performed slightly better than DVB sample due to combined positive effects of the enhanced conductivity and presence of cracks (Fig. 9) in the graphene layer facing the BPP; these cracks help expel excess liquid water.

Notably, samples containing pure graphene (SG and DG) consistently perform the worst across various humidity conditions. Despite graphene's enhanced electrical conductivity, its inferior mass transport properties offset this advantage. The very low content of micropores and mesopores in pure graphene samples (Fig. 7), compared to the Vulcan black samples, results in less retention of liquid water produced at the cathode catalyst layer, thus lowering the ionic conductivity of the membrane electrolyte. The composite samples containing higher graphene content (D_G100_VB100, D_GVB50_GVB50) also behaved similarly to the pure graphene samples due to decreased presence of micropores/mesopores in the MPL facing the catalyst layer, resulting in deteriorating performance due to poor retention of liquid water.

4. Conclusion

The impact of double-sided MPL coated GDLs, compared to conventional single-sided MPL coated GDLs, was investigated in terms of key characteristics and fuel cell performance. Two types of carbon for the MPL coatings were employed, Vulcan black and graphene. This was to evaluate the effects of introducing a novel material to the double-

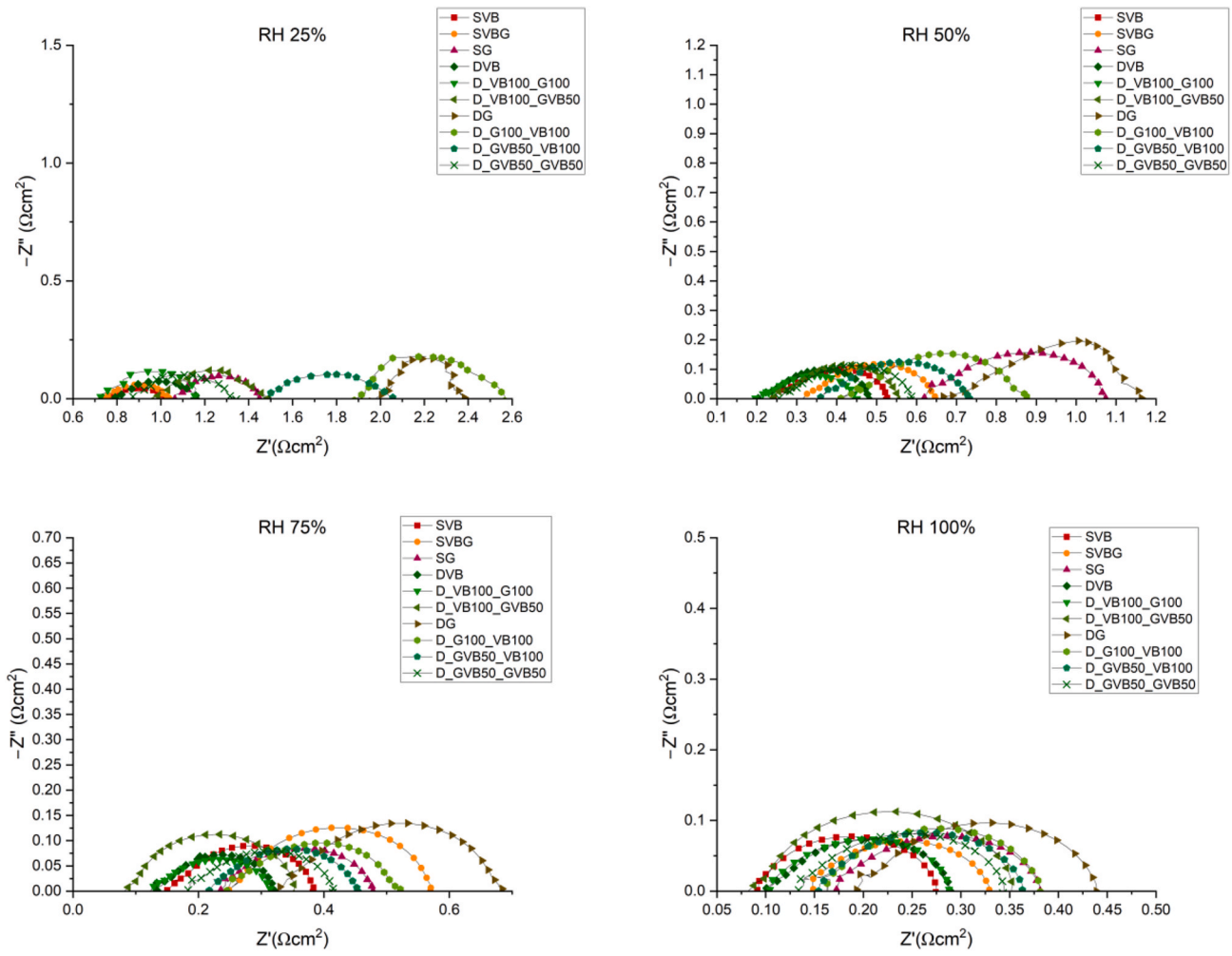

Fig. 12. The EIS curves of the fuel cell operating with the investigated samples at various humidity conditions (RH 25%, RH 50%, RH75% and RH 100%).

sided MPL coating and to see where improvements could be made. The MPL loadings applied to the surfaces of the GDL facing the catalyst layer and the bipolar plate were 1.25 and 0.25 mg/cm^2, respectively. The following key findings were made from the ex-situ and in-situ tests:

- Graphene samples displayed a higher gas permeability compared to Vulcan black samples, this is due to presence of a higher amount of cracks in the former samples. Expectedly, graphene samples displayed a higher in-plane electrical conductivity than the Vulcan black samples. Notably, the introduction of graphene at a 50% mixture with the Vulcan black results in a conductivity increase equivalent to that of a sample composed entirely of pure graphene. When analysing the contact angle, there is no notable variation. This suggests that contact angle is a factor more dependent on the PTFE content rather than the type carbon used in the MPL.
- MIP analysis showed that for all samples, the addition of Vulcan black MPLs created micropores and mesopores that are essential for efficient water removal at high current densities. Evidently, the double-sided Vulcan black MPL coating increased the amount of micropores and mesopores. On the other hand, the pure graphene samples produced the lowest content of micropores and mesopores. SEM micrographs of the samples showed that the graphene samples exhibited a higher number of surface cracks, while Vulcan carbon black samples displayed a smoother surface.
- Under low humidity conditions (25% RH), it is advisable to use single-sided MPL coated GDLs as the fuel cell, under these circumstances, is gas diffusion limited. These samples, compared to double-sided coated GDLs, offer lower diffusion paths and consequently lower mass transport resistance. Notably, single-sided Vulcan Black (SVB) and the single-sided composite of Vulcan Black and Graphene (SVBG) samples performed significantly better than single-sided graphene (SG) sample and this is due to the presence of micropores necessary to retain water for membrane humidification under low humidity conditions.
- Under relatively high humidity conditions ($\geq$50% RH), double-sided MPL coated GDLs generally performed better than single-sided MPL coated GDLs as they offer better electrical contact with the bipolar plates. Notably, the GDL with Vulcan Black MPL facing the CL and graphene MPL facing the BPP (D_VB100_G100) demonstrated the best overall performance. This configuration allowed for the correct water retention required for membrane humidification at the CL, yet it also facilitated the expulsion of excess water through the cracks available in the graphene MPL facing the BPP.

For future work, durability testing is essential for evaluating new fuel cell designs and materials, especially for the promising double-sided MPL-coated GDL. While this configuration shows potential, its long-term stability and performance under varied operational conditions need thorough assessment. Studying its degradation and robustness can help pinpoint areas for improvement [51]. Additionally, testing the durability of different carbon materials can highlight the most resilient options for sustained fuel cell use.

CRediT authorship contribution statement

F. Ruscillo: Writing – review & editing, Writing – original draft, Visualization, Methodology, Investigation, Formal analysis, Data curation, Conceptualization. **M.S. Ismail:** Writing – review & editing, Supervision, Formal analysis, Conceptualization. **Z.A.R. Gautama:** Investigation. **M. Nishihara:** Writing – review & editing, Supervision, Resources. **K.J. Hughes:** Writing – review & editing, Supervision. **D.B. Ingham:** Writing – review & editing, Supervision. **L. Ma:** Writing – review & editing, Supervision. **M. Pourkashanian:** Supervision, Project administration.

Declaration of competing interest

The authors declare that they have no known competing financial interests or personal relationships that could have appeared to influence the work reported in this paper.

Acknowledgements

The first author would like to acknowledge and thank the EPSRC Centre for Doctoral Training for Resilient Decarbonised Fuel Energy Systems (grant number EP/S022996/1) and the International Flame Research Foundation for their financial support. The authors would like to thank the Daiwa Anglo Japanese Foundation (Ref: 13826/14659) for supporting the first author's research visit to Kyushu University and the University of Kyushu for the use of their laboratory equipment and facilities.

Nomenclature

A	Cross Sectional Area (m^2)
C	Correction factor
d	Thickness (m)
i	Current density, (A/m^2)
I	Current (A)
k	Permeability, (m^2)
L	Thickness (m)
P	Pressure (Pa)
R	Electrical resistance (Ω)
T	Temperature (K)
t	Thickness (m)
μ	Fluid viscosity (Pa·s)
ρ	Electrical resistivity (Ω/m)
σ	Electrical conductivity (S/m)

Appendix A. Supplementary data

Supplementary data to this article can be found online at https://doi.org/10.1016/j.ijhydene.2024.12.094.

References

[1] Barbir F. PEM fuel cells: theory and practice. Elsevier Science & Technology; 2005.
[2] Aldakheel F, et al. Gas permeability, wettability and morphology of gas diffusion layers before and after performing a realistic ex-situ compression test. Renew Energy May 2020;151:1082–91. https://doi.org/10.1016/J.RENENE.2019.11.109.
[3] Lou M, Chen L, Lu K, Lin R. An experimental study on PEMFC water management based on the synergistic interaction of flow field and MPL. Int J Hydrogen Energy Jun. 2024;69:1246–54. https://doi.org/10.1016/J.IJHYDENE.2024.05.153.
[4] Ercelik M, Ismail MS, Hughes KJ, Ingham DB, Ma L, Pourkashanian M. X-ray CT-based numerical investigation of nickel foam-based GDLs under compression. Int J Hydrogen Energy Jan. 2024;50:1338–57. https://doi.org/10.1016/J.IJHYDENE.2023.07.001.
[5] Wang X, Liu YT, Zhang XF, Song H, Wu GP. Effects of the carbon black properties in gas diffusion layer on the performance of proton exchange membrane fuel cells. Int J Hydrogen Energy Aug. 2023;48(73):28528–38. https://doi.org/10.1016/J.IJHYDENE.2023.04.056.
[6] Sim J, Kang M, Min K. Effects of basic gas diffusion layer components on PEMFC performance with capillary pressure gradient. Int J Hydrogen Energy Aug. 2021;46(54):27731–48. https://doi.org/10.1016/J.IJHYDENE.2021.05.205.
[7] Park S, Lee JW, Popov BN. Effect of carbon loading in microporous layer on PEM fuel cell performance. J Power Sources Dec. 2006;163(1):357–63. https://doi.org/10.1016/J.JPOWSOUR.2006.09.020.
[8] Kitahara T, Konomi T, Nakajima H. Microporous layer coated gas diffusion layers for enhanced performance of polymer electrolyte fuel cells. J Power Sources Apr. 2010;195(8):2202–11. https://doi.org/10.1016/j.jpowsour.2009.10.089.
[9] Weber AZ, Newman J. Effects of microporous layers in polymer electrolyte fuel cells. J Electrochem Soc Mar. 2005;152(4):A677. https://doi.org/10.1149/1.1861194.
[10] Ismail MS, Damjanovic T, Ingham DB, Pourkashanian M, Westwood A. Effect of polytetrafluoroethylene-treatment and microporous layer-coating on the electrical conductivity of gas diffusion layers used in proton exchange membrane fuel cells. J Power Sources 2010;195:2700–8. https://doi.org/10.1016/j.jpowsour.2009.11.069.
[11] Antolini E, Passos RR, Ticianelli EA. Effects of the carbon powder characteristics in the cathode gas diffusion layer on the performance of polymer electrolyte fuel cells. 2002.
[12] Deevanhxay P, Sasabe T, Tsushima S, Hirai S. Effect of liquid water distribution in gas diffusion media with and without microporous layer on PEM fuel cell performance. 2013. https://doi.org/10.1016/j.elecom.2013.07.001.
[13] Kitahara T, Nakajima H, Mori K. Hydrophilic and hydrophobic double microporous layer coated gas diffusion layer for enhancing performance of polymer electrolyte fuel cells under no-humidification at the cathode. J Power Sources Feb. 2012;199:29–36. https://doi.org/10.1016/J.JPOWSOUR.2011.10.002.
[14] Gostick JT, Ioannidis MA, Fowler MW, Pritzker MD. On the role of the microporous layer in PEMFC operation. Electrochem Commun Mar. 2009;11(3):576–9. https://doi.org/10.1016/J.ELECOM.2008.12.053.
[15] Bednarek T, Tsotridis G. Issues associated with modelling of proton exchange membrane fuel cell by computational fluid dynamics. J Power Sources Mar. 2017;343:550–63. https://doi.org/10.1016/J.JPOWSOUR.2017.01.059.
[16] Okereke IC, Ismail MS, Ingham DB, Hughes K, Ma L, Pourkashanian M. Single- and double-sided coated gas diffusion layers used in polymer electrolyte fuel cells: a numerical study. Energies Jun. 2023;16(11):4363. https://doi.org/10.3390/EN16114363/S1.
[17] Wang X, et al. A bi-functional micro-porous layer with composite carbon black for PEM fuel cells. J Power Sources 2006;162:474–9. https://doi.org/10.1016/j.jpowsour.2006.06.064.
[18] Chang HM, Chang MH. Effect of gas diffusion layer with double-side microporous layer coating on polymer electrolyte membrane fuel cell performance. J Fuel Cell Sci Technol Apr. 2013;10(2). https://doi.org/10.1115/1.4023841.
[19] Huang G-M, Chang M-H. Effect of gas diffusion layer with double-side microporous layer coating on proton exchange membrane fuel cell performance under different air inlet relative humidity [Online]. Available:www.electrochemsci.org, ; 2014.
[20] Nitta I, Himanen O, Mikkola M. Contact resistance between gas diffusion layer and catalyst layer of PEM fuel cell. 2007. https://doi.org/10.1016/j.elecom.2007.10.029.
[21] H. Zamora, P. Cañizares, M. A. Rodrigo, and J. Lobato, "Improving of micro porous layer based on advanced carbon materials for high temperature proton exchange membrane fuel cell electrodes," doi: 10.1002/fuce.201400139.

[22] Lee FC, et al. Alternative architectures and materials for PEMFC gas diffusion layers: a review and outlook. Renew Sustain Energy Rev Sep. 2022;166:112640. https://doi.org/10.1016/J.RSER.2022.112640.
[23] A. Ta heri Najafabadi, M. J. Leeuwner, D. P. avid Wilkinson, and dLG yenge, "Electrochemically produced graphene for microporous layers in fuel cells," doi: 10.1002/cssc.201600351.
[24] Leeuwner MJ, Wilkinson DP, Gyenge EL. Novel graphene foam microporous layers for PEM fuel cells: interfacial characteristics and comparative performance. 2015. https://doi.org/10.1002/fuce.201500031.
[25] Ozden A, Shahgaldi S, Li X, Hamdullahpur F. A graphene-based microporous layer for proton exchange membrane fuel cells: characterization and performance comparison. 2018. https://doi.org/10.1016/j.renene.2018.03.065.
[26] Ozden A, Shahgaldi S, Zhao J, Li X, Hamdullahpur F. Assessment of graphene as an alternative microporous layer material for proton exchange membrane fuel cells. 2017. https://doi.org/10.1016/j.fuel.2017.11.109.
[27] Mariani M, Latorrata S, Patrignani S, Gallo Stampino P, Dotelli G. Characterization of novel graphene-based microporous layers for Polymer Electrolyte Membrane Fuel Cells operating under low humidity and high temperature. Int J Hydrogen Energy Feb. 2020;45(11):7046–58. https://doi.org/10.1016/J.IJHYDENE.2019.12.213.
[28] Leeuwner MJ, Patra A, Wilkinson DP, Gyenge EL. Graphene and reduced graphene oxide based microporous layers for high-performance proton-exchange membrane fuel cells under varied humidity operation. J Power Sources May 2019;423:192–202. https://doi.org/10.1016/J.JPOWSOUR.2019.03.048.
[29] Lee FC, et al. Optimisation and characterisation of graphene-based microporous layers for polymer electrolyte membrane fuel cells. Int J Hydrogen Energy May 2023. https://doi.org/10.1016/J.IJHYDENE.2023.05.003.
[30] Su H, Hu YH. Recent advances in graphene-based materials for fuel cell applications. Energy Sci Eng Jul. 2021;9(7):958–83. https://doi.org/10.1002/ESE3.833.
[31] Park S, et al. Design of graphene sheets-supported Pt catalyst layer in PEM fuel cells. Electrochem Commun Mar. 2011;13(3):258–61. https://doi.org/10.1016/J.ELECOM.2010.12.028.
[32] Ferreira RB, Falcão DS, Oliveira VB, Pinto AMFR. Experimental study on the membrane electrode assembly of a proton exchange membrane fuel cell: effects of microporous layer, membrane thickness and gas diffusion layer hydrophobic treatment. Electrochim Acta Jan. 2017;224:337–45. https://doi.org/10.1016/J.ELECTACTA.2016.12.074.
[33] Zhou P, Wu CW, Ma GJ. Contact resistance prediction and structure optimization of bipolar plates. J Power Sources Sep. 2006;159(2):1115–22. https://doi.org/10.1016/J.JPOWSOUR.2005.12.080.
[34] Nitta I, Hottinen T, Himanen O, Mikkola M. Inhomogeneous compression of PEMFC gas diffusion layer Part I. Experimental. J Power Sources 2007;171:26–36. https://doi.org/10.1016/j.jpowsour.2006.10.076.
[35] Sadeghi E, Djilali N, Bahrami M. Effective thermal conductivity and thermal contact resistance of gas diffusion layers in proton exchange membrane fuel cells. Part 2: hysteresis effect under cyclic compressive load. J Power Sources Dec. 2010;195(24):8104–9. https://doi.org/10.1016/J.JPOWSOUR.2010.07.051.
[36] Ruscillo F, et al. Characterisation of novel and high performing double-sided microporous-layers-coated gas diffusion layers for polymer electrolyte membrane fuel cells. Energies Nov. 2023;16(22):7601. https://doi.org/10.3390/EN16227601. 2023, Vol. 16, Page 7601.
[37] Smits FM. Measurement of sheet resistivities with the four-point probe. Bell Syst. Tech. J. 1958;37(3):711–8. https://doi.org/10.1002/J.1538-7305.1958.TB03883.X.
[38] Ismail MS, Borman D, Damjanovic T, Ingham DB, Pourkashanian M. On the through-plane permeability of microporous layer-coated gas diffusion layers used in proton exchange membrane fuel cells. Int J Hydrogen Energy Aug. 2011;36(16):10392–402. https://doi.org/10.1016/J.IJHYDENE.2010.09.012.
[39] Orogbemi O, Ingham D, Ismail M, Hughes K, Ma L, Pourkashanian M. Through-plane gas permeability of gas diffusion layers and microporous layer: effects of carbon loading and sintering. 2017. https://doi.org/10.1016/j.joei.2016.11.008.
[40] Ozden A, Alaefour IE, Shahgaldi S, Li X, Colpan CO, Hamdullahpur F. Gas diffusion layers for PEM fuel cells: ex- and in-situ characterization. Exergetic, Energ. Environ. Dimens. 2018:695–727. https://doi.org/10.1016/B978-0-12-813734-5.00040-8.
[41] Giesche H. Mercury porosimetry: a general (practical) overview. Part Part Syst Char Jun. 2006;23(1):9–19. https://doi.org/10.1002/PPSC.200601009.
[42] Yang Y, Zhou X, Li B, Zhang C. Recent progress of the gas diffusion layer in proton exchange membrane fuel cells: material and structure designs of microporous layer. Int J Hydrogen Energy Jan. 2021;46(5):4259–82. https://doi.org/10.1016/J.IJHYDENE.2020.10.185.
[43] El-Kharouf A, Mason TJ, Brett DJL, Pollet BG. Ex-situ characterisation of gas diffusion layers for proton exchange membrane fuel cells. J Power Sources Nov. 2012;218:393–404. https://doi.org/10.1016/J.JPOWSOUR.2012.06.099.
[44] Lee HK, Park JH, Kim DY, Lee TH. A study on the characteristics of the diffusion layer thickness and porosity of the PEMFC. J Power Sources May 2004;131(1–2):200–6. https://doi.org/10.1016/J.JPOWSOUR.2003.12.039.
[45] Fang Z, Star AG, Fuller TF. Effect of carbon corrosion on wettability of PEM fuel cell electrodes. J Electrochem Soc 2019;166(12):F709–15. https://doi.org/10.1149/2.0231912JES.
[46] Mench M, Kumbur EC. Polymer electrolyte fuel cell degradation. Academic Press; 2011.
[47] Chen W, Jiang F. Impact of PTFE content and distribution on liquidegas flow in PEMFC carbon paper gas distribution layer: 3D lattice Boltzmann simulations. 2016. https://doi.org/10.1016/j.ijhydene.2016.02.159.
[48] Litster S, Sinton D, Djilali N. Ex situ visualization of liquid water transport in PEM fuel cell gas diffusion layers. J Power Sources Mar. 2006;154(1):95–105. https://doi.org/10.1016/J.JPOWSOUR.2005.03.199.
[49] Chen Z, et al. Crack evolution during the film drying process of fuel cell microporous layer ink. Colloids Surfaces A Physicochem. Eng. Asp. Oct. 2022;650:129283. https://doi.org/10.1016/J.COLSURFA.2022.129283.
[50] Markötter H, et al. Influence of cracks in the microporous layer on the water distribution in a PEM fuel cell investigated by synchrotron radiography. 2013. https://doi.org/10.1016/j.elecom.2013.04.006.
[51] Ren P, Pei P, Li Y, Wu Z, Chen D, Huang S. Degradation mechanisms of proton exchange membrane fuel cell under typical automotive operating conditions. Prog Energy Combust Sci Sep. 2020;80:100859. https://doi.org/10.1016/J.PECS.2020.100859.